ELSEVIER

NeuroImage

www.elsevier.com/locate/ynimg
NeuroImage 21 (2004) 914–923

Differential effects of testosterone on neuronal populations and their connections in a sensorimotor brain nucleus controlling song production in songbirds: a manganese enhanced-magnetic resonance imaging study

Vincent Van Meir,[a,*] Marleen Verhoye,[a] Philippe Absil,[b] Marcel Eens,[b] Jacques Balthazart,[c] and Annemie Van der Linden[a]

[a] *Bio-Imaging Laboratory, Department of Biomedical Sciences, University of Antwerp, B-2020 Antwerp, Belgium*
[b] *Department of Biology, University of Antwerp, B-2610 Wilrijk, Belgium*
[c] *Center for Cellular and Molecular Neurobiology, Research Group in Behavioral Neuroendocrinology, University of Liège, B-4020 Liège, Belgium*

Received 19 June 2003; revised 8 September 2003; accepted 6 October 2003

Nucleus HVC (formerly called high vocal center) of songbirds contains two types of projecting neurons connecting HVC respectively to the nucleus robustus archistriatalis, RA, or to area X. These two neuron classes exhibit multiple neurochemical differences and are differentially replaced by new neurons during adult life: high rates of neuronal replacement are observed in RA-projecting neurons only. The activity of these two types of neurons may also be modulated differentially by steroids. We analyzed by magnetic resonance imaging the effect of testosterone on the volume of RA and area X and on the dynamics of Mn^{2+} accumulation in RA and area X of female starlings that had been injected with $MnCl_2$ through a permanent cannula implanted in HVC. Repeated visualization 6 weeks apart (before and after testosterone treatment) identified a volume increase of both nuclei in testosterone-treated birds associated with a concomitant decrease in controls. Following testosterone treatment, the total amount of Mn^{2+} transported to RA and area X increased but the dynamics of accumulation, reflecting in part the activity of HVC neurons, was specifically altered in area X but not in RA. These data indicate that testosterone differentially affects the RA- and area X-projecting neurons in HVC. Manganese-enhanced magnetic resonance imaging (ME-MRI) thus provides repeated measures of connected brain areas and demonstrates testosterone-dependent regionally specific changes in brain activity and functional connectivity. The slow time scales investigated by this technique (compared to functional MRI) appear ideally suited for characterizing slow processes such as those involved in brain plasticity and learning.

Keywords: Starling; Songbird; Song control nuclei; HVC; RA; Area X; Brain plasticity; Testosterone; Manganese enhanced-MRI

Introduction

Songbirds are one of the few groups of vertebrates that evolved a vocal communication system, which is based on the production of songs of various complexities. These songs play a key role in social (sexual, aggressive) interactions and are learned during ontogeny. In songbird species that live in the temperate zone, the structure and function of songs also changes seasonally. During the phylogenetic evolution that led to songbirds, several telencephalic brain regions became part of a spatially organized neuronal circuitry along with the ability of song learning and song production; these brain regions are called song control nuclei (Brenowitz et al., 1997; Fig. 1). In response to changes in day length and plasma testosterone, the song control nuclei of songbirds exhibit among the largest morphological changes that have been described in the brain of warm-blooded vertebrates (Tramontin and Brenowitz, 2000). A high level of neuronal replacement, associated with an active neurogenesis also takes place in some of these nuclei even in adult birds, which makes them an outstanding model to study brain plasticity in vertebrates. HVC (the song control nucleus formerly known as high vocal center) is an important sensory motor region that serves as a relay center within the vocal network connecting the brain areas involved in hearing, song production and vocal learning in songbirds. It contains three distinct types of neurons from which two project respectively to the nucleus robustus archistriatalis, RA, or to area X. The third type can be identified as interneurons. All three neuron types show strong electrical responses both during song production and during auditory stimulation with songs (Mooney et al., 2002).

The two types of projection neurons are part of two brain circuits that play a critical role in the production of song (RA-projecting neurons) or its acquisition in juveniles and stability in adults (X-projecting neurons) (Brainard and Doupe, 2000a,b; Hessler and Doupe, 1999; Jarvis et al., 1998; Nottebohm et al., 1976; Scharff and Nottebohm, 1991; Yu and Margoliash, 1996). RA-projecting neurons are part of a motor pathway that controls

* Corresponding author. Bio-Imaging Laboratory, UA, Department of Biomedical Sciences, University of Antwerp, Groenenborgerlaan 171-Gebouw V, B-2020 Antwerp, Belgium. Fax: +32-3-218-02-33.
E-mail address: vincent.vanmeir@ua.ac.be (V. Van Meir).
Available online on ScienceDirect (www.sciencedirect.com.)

1053-8119/$ - see front matter © 2004 Elsevier Inc. All rights reserved.
doi:10.1016/j.neuroimage.2003.10.007

the activity of the syrinx, the sound-producing organ in birds, and of medullary nuclei that synchronize respiration with song production (Wild, 1997). The X-projecting neurons, in contrast, belong to the so-called anterior forebrain pathway that is required for song learning but also plays a key role in maintaining song stability in adulthood (Brainard and Doupe, 2000a,b). This pathway includes the area X in the avian homologue of the mammalian basal ganglia (the lobus parolfactorius or caudate–putamen in mammals) and it is therefore not surprising that this circuit plays a role in the coordination of fine motor actions. It is well known that in human neurodegenerative diseases such as Parkinson's disease, leading to alterations of the basal ganglia circuits, are associated with severe problems of motor coordination.

Most studies of the song system have relied so far on histological techniques that require the sacrifice of the experimental subjects and therefore prevent the use of birds as their own controls in successive measurements. However, recent advances in magnetic resonance imaging (MRI) techniques have allowed visualization and accurate delineation of the two monosynaptic targets of HVC, RA and area X, by application of an in vivo tract-tracing technique based on the injection of paramagnetic Mn^{2+} into HVC. This technique, which uses Mn^{2+} as a calcium analogue, is known as manganese-enhanced (ME)-MRI. Previous work had used Mn^{2+} to identify activated brain regions, taking advantage of the tract tracing properties of this ion (Pautler and Koretsky, 2002) or after its intravenous infusion associated with a pharmacological opening of the blood–brain barrier (Aoki et al., 2002; Duong et al., 2000; Lin and Koretsky, 1997). In addition, our work that analyzed the dynamics of Mn^{2+} accumulation in the two target nuclei of HVC revealed functional sex differences between the RA- and area X-projecting HVC neurons (Van der Linden et al., 2002). This approach, that we called dynamic ME-MRI, opens new perspectives for the study of brain plasticity in particular for long-term studies of morphological and functional responses of specific brain circuits to changes in endocrine conditions. We used here repeated dynamic ME-MRI in a well-characterized neuronal system to assess the potential of this technique through the study in individual birds of the long-term effects of testosterone on the song control system of female starlings. Repeated visualization and monitoring of the dynamics of Mn^{2+} accumulation in RA and area X demonstrates testosterone-dependent regionally specific changes in brain activity and functional connectivity.

Materials and methods

Experimental setup

Ten first-year female starlings were caught in the wild during the winter before February and housed in two indoor cages (1.40 × 2.20 × 2.10 m) on a stable 10:14-h light–dark cycle, that was selected to maintain birds in a durable state of photosensitivity. All birds were studied by MRI for the first time between March 15 and April 30, 2001. One or two days after the first ME-MRI measurement, subjects were implanted subcutaneously in the neck region with one 15-mm long Silastic™ capsule [Degania Silicone, inner diameter (id) 1.47 mm, outer diameter (od) 1.96 mm] filled with crystalline testosterone (Sigma, St. Louis, MO) (testosterone-treated birds, $n = 5$) or left empty (control birds, $n = 5$). Birds were studied by MRI again 5 to 6 weeks after the treatment. All experimental procedures were approved by the Committee on Animal Care and Use at the University of Antwerp, Belgium.

Testosterone assay

The day before or after each ME-MRI measurement, a blood sample (250–400 μl) was taken from the brachial vein into heparinized haematocrit capillary tubes, centrifuged and the plasma stored at −25°C. Testosterone levels were determined in all samples using an iodine-125 double-antibody assay (ICN Biomedicals, Inc., Costa Mesa, CA) (Eens et al., 2000) previously validated for use in starlings (Duffy et al., 2000).

Cannula implantation

To allow repeated and reproducible injections of $MnCl_2$, one plastic cannula (id 0.39 μm, od 0.69 μm; Plastics One, Inc., Roanoke, VA) was implanted in the right HVC of each bird that was anaesthetized as described before (Van der Linden et al., 2002). Briefly, birds were first anaesthetized with an intramuscular injection of 5 ml/kg of a mixture containing 0.33 ml xylazine (Rompun: 20 mg/ml), 2.10 ml ketamine (Ketalar: 50 mg/ml) and 4.33 ml saline solution. Anesthesia was maintained by administration of one fifth of the initial dose every 30 min through a catheter positioned in the chest muscle. The head of the animal was fixed in a stereotaxic device with the beak positioned 45° under the horizontal plane of the ear bars. An incision was made in the skin and the skull opened at the appropriate coordinates. The V-shape formed by the vena cerebralis dorsocaudalis and two branches of the sinus transversus at the border of the two telencephalic lobes was taken as zero point for positioning the cannula. From this point, the cannula coordinates were +3.0 mm lateral to the right and −0.7 mm deep. The cannula was fixed to the skull with dental cement (Dentalbiolux, Int., Brussels, Belgium), the skin was sutured and the bird was allowed to recover. When not used for injections, cannulae were closed by a dummy insert (Plastics One) The first ME-MRI measures were done at least 5 days later.

ME-MRI protocol

The anaesthetized subject was immobilized in a nonmagnetic Teflon™ stereotaxic head holder combined with a radio frequency receiver surface antenna (diameter 20 mm) and a headphone transmitter antenna (diameter 45 mm). Two hundred nanoliter of a 10 mM $MnCl_2$ solution was injected over a period of 10 min during the MRI acquisition with the bird positioned inside the magnet. For this purpose we used an internal cannula (fused silica: id 0.152 μm, od 0.36 μm) (Plastics One) that fitted into the plastic cannula and was connected by a 2 m long PE50 tubing (id 580 μm, od 965 μm) (Intramedic, Sparks, MD) to a pressure injection pump (Apparatebeau injector, B. Braun, Melsungen, Germany) positioned outside the magnet. This allowed monitoring quantitatively the dynamics of the Mn^{2+} accumulation in RA and area X starting from a control situation before Mn^{2+} was present in the brain. $MnCl_2$ was injected, between two layers of mineral oil (sandwich technique), which ensures a reproducible injection volume.

Magnetic resonance (MR) images were acquired on a 7 T horizontal bore MR microscope (SMIS, MRRS, Guildford, UK), provided with shielded gradients (8 cm width, maximal strength = 0.1 T/m). The dynamic of the Mn^{2+} accumulation was studied by

T_1-weighted multislice spin echo images (FOV = 30 mm, acquisition matrix = 256 × 128, image matrix = 256 × 256, slice thickness = 0.8 mm) as described in Van der Linden et al. (2002). After acquisition of a set of control images, $MnCl_2$ was injected in the cannulated HVC. Two sets of five coronal slices (one through HVC and RA, one through area X) were then acquired every 15 min for up to 6–7 h after injection.

The volumes of RA and area X were determined on coronal 3D spin echo T_1-weighted images obtained 8 h after $MnCl_2$ injection as described earlier (Van der Linden et al., 2002) except for the FOV = 25 × 25 × 25 mm, the image matrix = 256 × 256 × 256 and the total acquisition time = 90 min. Each MRI experiment took approximately 10–12 h. During the whole experiment starlings were kept anaesthetized as described above (see also Van der Linden et al., 2002), except that the anesthetic was infused in the chest muscle at a constant rate of 0.15 ml/h. Body temperature was continuously monitored and kept within a narrow range (40–41 °C; Van der Linden et al., 2002).

ME-MRI data processing

Dynamic ME-MRI

RA and area X were segmented on the T_1-weighted multislice images obtained 6 h after injection. Mean signal intensity was determined within the defined regions of interest and in an adjacent control area in images collected every 15 min starting before the injection for up to 6–7 h after the injection. Changes in relative signal intensity were then plotted as a function of time and fitted by nonlinear regression to a sigmoid curve to define the kinetics: the maximal signal intensity (SI_{max}), the time required to reach 50% of this maximum (T_{50}) and the *n* coefficient that describes the shape of the curve (Van der Linden et al., 2002). When a sigmoid curve is used to describe a complex (allosteric) kinetics in enzymology, *n* reflects the index of cooperativity and provides a measure of the numbers of active sites in an enzyme that participate to the catalysis of the reaction (number of substrate binding sites). *n* therefore provides by analogy a measure of the complexity of the processes involved in the uptake, transport and accumulation of Mn^{2+} in the targets even if the cellular nature of these processes cannot be inferred from the value of this coefficient.

Nucleus volume reconstruction

RA and area X were delineated on 3D coronal MRI sections and the total number of pixels in the nuclei was multiplied by the resolution of the image (1 voxel = 9.3×10^{-4} mm^3) to obtain the volume of the nucleus. The total amount of manganese transported to area X and RA was calculated as the product of the maximal average signal intensity (SI_{max}) by the volume of the nucleus (Van der Linden et al., 2002).

Histological measurements

After the last MRI acquisition, birds were decapitated, their brains removed, frozen on dry ice and stored at −70 °C until used for histological analyses. Brains were sectioned at 50 μm thickness in the coronal plane with a cryostat. Sections were stained for Nissl bodies with toluidine blue. The volumes of RA and area X on the cannulated and noncannulated side were reconstructed with the help of the NIH-Image Program (version 1.52; Wayne Rasband; NIH, Bethesda, MD) on a Macintosh computer equipped with a CCD camera mounted on a microscope using objective ×10 (for RA) or ×5 (for area X). The area of interest was measured in sections collected every 150 μm, these measurements were summed and multiplied by 150 μm.

Statistics

All data were analyzed by mixed two-way ANOVA with the experimental groups as independent factor and multiple measures in a same subject as repeated factor. In all analyses, effects were considered significant for $P \leq 0.05$. Results of these analyses are summarized in the text by providing the *F* values (ratios of variance related to the factor under study versus the residual unexplained variance), the associated degrees of freedom (in parentheses after the *F* values) and the corresponding probabilities. These results are provided for each main effect and for the interaction between factors in case of multifactorial ANOVA (see Steel and Torrie, 1980 for detail on statistical techniques). All values presented are means ± SEM.

Results

Serum testosterone concentrations

Analysis of plasma testosterone levels at the beginning and end of the experiment identified a significant group difference (testosterone vs. control; $F(1,8) = 5.586$, $P = 0.0457$), as well as effects of time of sampling (before vs. after implant; $F(1,8) = 6.106$, $P = 0.0387$) and of the interaction between the two factors [$F(1,8) = 7.143$, $P = 0.0282$]. In the testosterone group, testosterone levels were higher after (3.31 ± 1.26 ng/ml) than before (0.04 ± 0.01 ng/ml) treatment but no change was observed in control birds (before:

Table 1
Statistical analysis of the volumes and kinetic parameters describing Mn^{2+} accumulation in RA and area X of control and testosterone-treated female starlings

	Group		Time		Interaction	
	F(1,8)	*P*	*F*(1,8)	*P*	*F*(1,8)	*P*
RA						
Volume	0.001	0.9874	0.129	0.7291	10.818	**0.0110**
SI_{max}	0.453	0.5199	0.105	0.7543	2.789	0.1335
n	1.508	0.2543	0.801	0.3970	0.760	0.4086
T_{50}	0.487	0.5050	1.513	0.2536	1.399	0.2708
SI_{max} × volume	0.023	0.8838	0.175	0.6863	5.869	**0.0417**
Area X						
Volume	0.001	0.9781	1.948	0.2004	8.057	**0.0219**
SI_{max}	6.899	**0.0303**	1.176	0.3098	4.998	0.0588
n	0.710	0.4240	1.357	0.2778	6.326	**0.0361**
T_{50}	0.435	0.5277	3.136	0.1145	2.159	0.1799
SI_{max} × volume	5.830	**0.0422**	1.548	0.2486	5.662	**0.0446**

Data were analyzed by two-way ANOVA with the experimental groups (control vs. testosterone-treated) and the two time points (before and after treatment) as independent variables. For each dependent variable considered, the table presents the degrees of freedom, *F* and *P* values associated with the two main effects (groups, time) and their interaction. *P*-values indicated in bold are considered significant ($P < 0.05$).

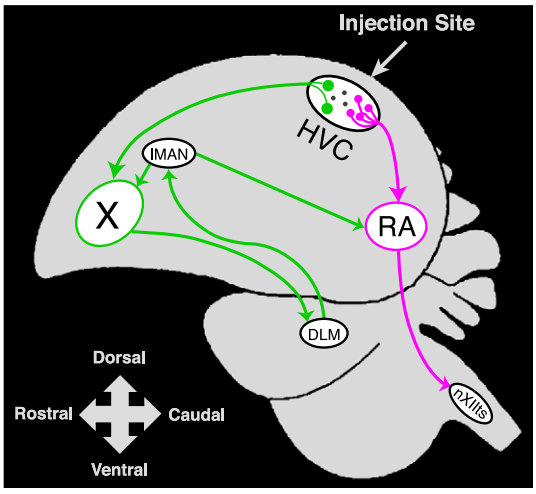

Fig. 1. Schematic sagittal view on the song control system. The green arrows represent the anterior forebrain pathway that starts in HVC and projects to area X → DLM → lMAN. Individual cells in lMAN project both to area X and to the RA. The pink arrows indicate the motor pathway that projects from HVC directly to RA and further to nXIIts. Notice that the two pathways originate from distinct cell populations within HVC. A third population of neurons in HVC consists of interneurons, here indicated in gray. Manganese was repeatedly injected into HVC to evaluate the physiological modulation of the two pathways upon testosterone treatment.

0.23 ± 0.17; after: 0.10 ± 0.03 ng/ml). Initial plasma testosterone levels were not different between these two groups [$F(1,8) = 1.206$, $P = 0.304$] but they were very different at the end of the experiment [$F(1,8) = 6.458$, $P = 0.0346$]. The testosterone levels observed in the testosterone group after treatment are similar to the levels of free ranging males during the breeding season (Ball and Wingfield, 1987).

Impact of cannulation on HVC targets

To analyze the potential impact of the cannula on HVC targets, birds were sacrificed at the end of the ME-MRI experiments and their brains were processed by histological techniques to determine the volumes of RA and area X in both the right (cannulated) and the left (noncannulated) hemisphere. Volumes were accurately reconstructed in three control and five testosterone-treated birds among birds used for the ME-MRI experiments plus two additional subjects treated with testosterone in similar conditions. Two way ANOVA with one repeated factor (brain side) identified no difference in the volume of RA or area X between the right and left side [RA: $F(1,8) = 0.005$, $P = 0.9431$; area X: $F(1,6) = 0.070$, $P = 0.8000$] and no interaction between groups and brain side [RA: $F(1,8) = 0.137$, $P = 0.7210$; area X: $F(1,6) = 0.785$, $P = 0.4098$]. Thus the implantation of a cannula into HVC does not affect RA and area X volumes.

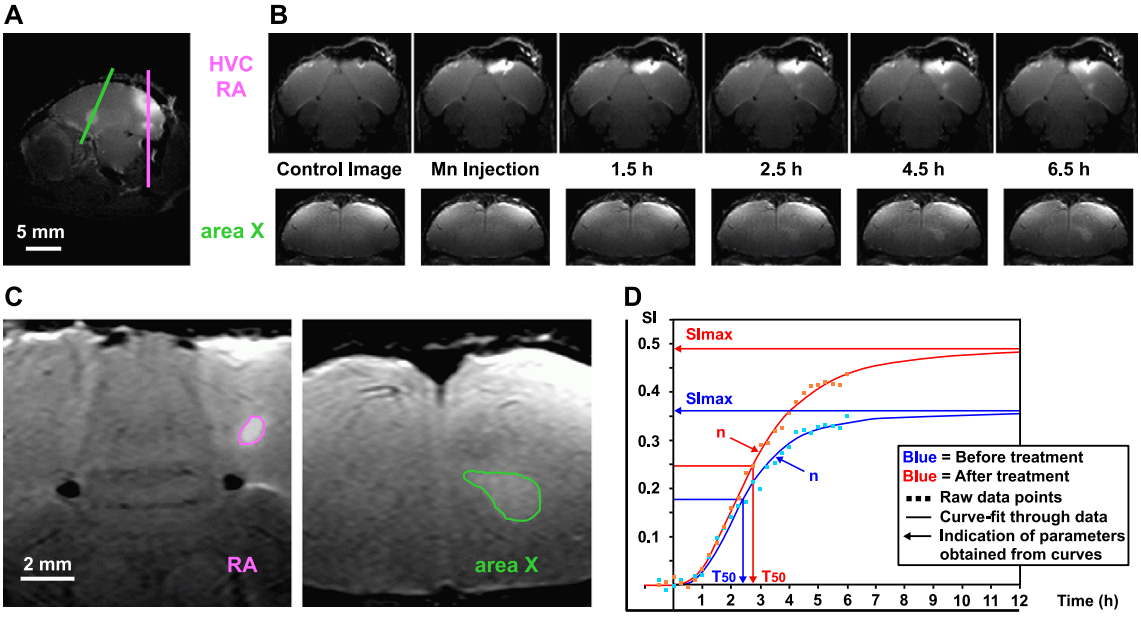

Fig. 2. Illustration of the dynamic ME-MRI images and subsequent data processing. Panel A indicates on a sagittal ME-MR image the position of the coronal slices covering area X (green line) and RA (pink line). Panel B illustrates the Mn^{2+} uptake in RA and area X following $MnCl_2$ stereotaxic injection into HVC. A control image was obtained before the $MnCl_2$ injection. Subsequently the increase in signal intensity due to Mn^{2+}-ions in RA (top) and area X (bottom) was followed on coronal brain sections (slice thickness = 0.8 mm). Both nuclei were delineated as shown in panel C. The pictures shown in this panel are obtained from a 3D dataset recorded immediately after the acquisition of the dynamic ME-MR images and have an in plane resolution of 100 μm and a slice thickness of 100 μm. They show, respectively RA (left) delineated in pink and area X (right) delineated in green. Further data processing is explained in Panel D. SI increases in RA of one individual, indicated by the small squares, is shown before (blue) and after (red) treatment with testosterone. Through each set of data points a sigmoid curve is fitted by nonlinear regression; it is characterized by three parameters SI_{max}, n and T_{50} which are indicated on the figure. SI_{max} is the maximal SI determined by the asymptote of the curve. T_{50} is the time point when half the SI of SI_{max} is reached. Finally, n is a parameter which describes the overall shape of the curve (see text for further explanation). The data were analyzed by comparison of each parameter in one individual before and after a treatment with either testosterone or a placebo (control) implant.

The volume of both nuclei was numerically larger in testosterone-treated than in control birds (RA: 0.454 ± 0.033 vs. 0.334 ± 0.013 mm^3; area X: 2.395 ± 0.391 vs. 1.434 ± 0.168 mm^3) but the difference did not reach statistical significance [RA: $F(1,8) = 5.095$, $P = 0.0540$; area X: $F(1,6) = 1.791$, $P = 0.2293$].

Effects of testosterone on RA and area X volumes measured by ME-MRI

No overall difference was detected by two way ANOVA [factors = treatment (testosterone vs. control) and repeated measures (before vs. after testosterone)] in the volume of RA or area X between testosterone-treated and control birds and no overall change in these volumes took place between the two successive measures performed by ME-MRI (no effect of the two main factors in the ANOVA; see Fig. 3 and Table 1). There was however a significant interaction between these factors [RA: $F(1,8) = 10.818$, $P = 0.0110$, X: $F(1,8) = 8.057$, $P = 0.0219$] reflecting the volume increases in testosterone-treated birds (RA: 50.2 ± 20.8%, X: 19.6 ± 7.6%) and concomitant decreases in control subjects (RA: −25.6 ± 11.5%, X: −5.7% ± 4.6%) (Fig. 3, top). Due to these changes in opposite directions observed in testosterone-treated and control birds, *t* tests revealed no difference between the two groups in the first or second set of measures.

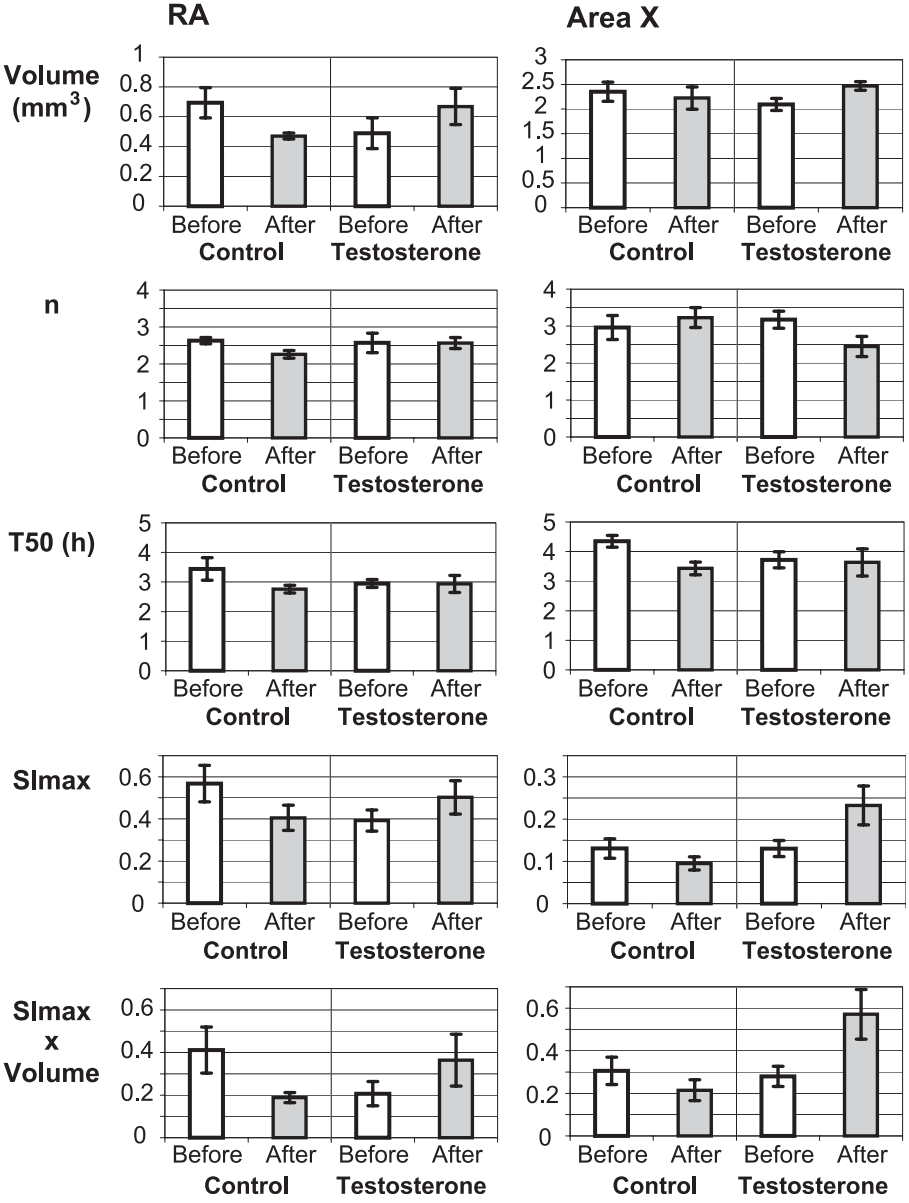

Fig. 3. Repeated measurements by ME-MRI of the volumes of RA and area X and of the Mn^{2+} accumulation in these nuclei. The figure presents the average volumes with standard error that were measured and the average values with standard error of the parameters defining the sigmoid curves that were fitted on the data points describing the Mn^{2+} accumulation in RA (left) and area X (right). White and gray bars represent the measures before and after treatment, respectively, with a control ($n = 5$) or testosterone ($n = 5$) implant.

Kinetics of Mn^{2+} accumulation in RA and area X

Because Mn^{2+} is a calcium analogue that enters HVC neurons largely as a function of their electrical activity, the kinetics of Mn^{2+} accumulation in RA and area X reflects the activity of the RA- and area X-projecting HVC neurons, respectively. The two sets of 5 coronal slices (one through HVC and RA, one through area X) acquired every 15 min during 6–7 h after the injection of Mn^{2+} into HVC provided a clear visualization of these processes (Fig. 2).

Changes in the activity or density of these projections following testosterone treatment were estimated by the analysis of three parameters (SI_{max}, n and T_{50}) describing the sigmoid curve fitted to the observed time-dependent changes in the signal intensity in RA and area X. The rate of accumulation of Mn^{2+} in RA was not affected by testosterone and did not change in time between the first and second ME-MRI measures that were taken approximately 5 to 6 weeks apart (Figs. 3 and 4). Two-way ANOVA of the three parameters describing these accumulation curves detected no significant effects of the treatment, of the repeated measure and of their interaction (all $P > 0.25$, see Table 1).

Significant changes were, in contrast, observed in parameters describing Mn^{2+} accumulation in area X. An overall group difference between testosterone-treated and control birds was observed for SI_{max} (Fig. 3). During the experiment, this intensity tended to decrease in control subjects but increased in testosterone-treated birds which resulted in a nearly significant interaction ($P = 0.0588$) between the two factors (groups and time) in the ANOVA. The maximal intensity of the signal in testosterone-treated birds (after treatment) was almost twice higher than the intensity in control birds at the same time.

In addition, the shape of the curve (n factor) leading to this differential accumulation of Mn^{2+} changed differentially in time in

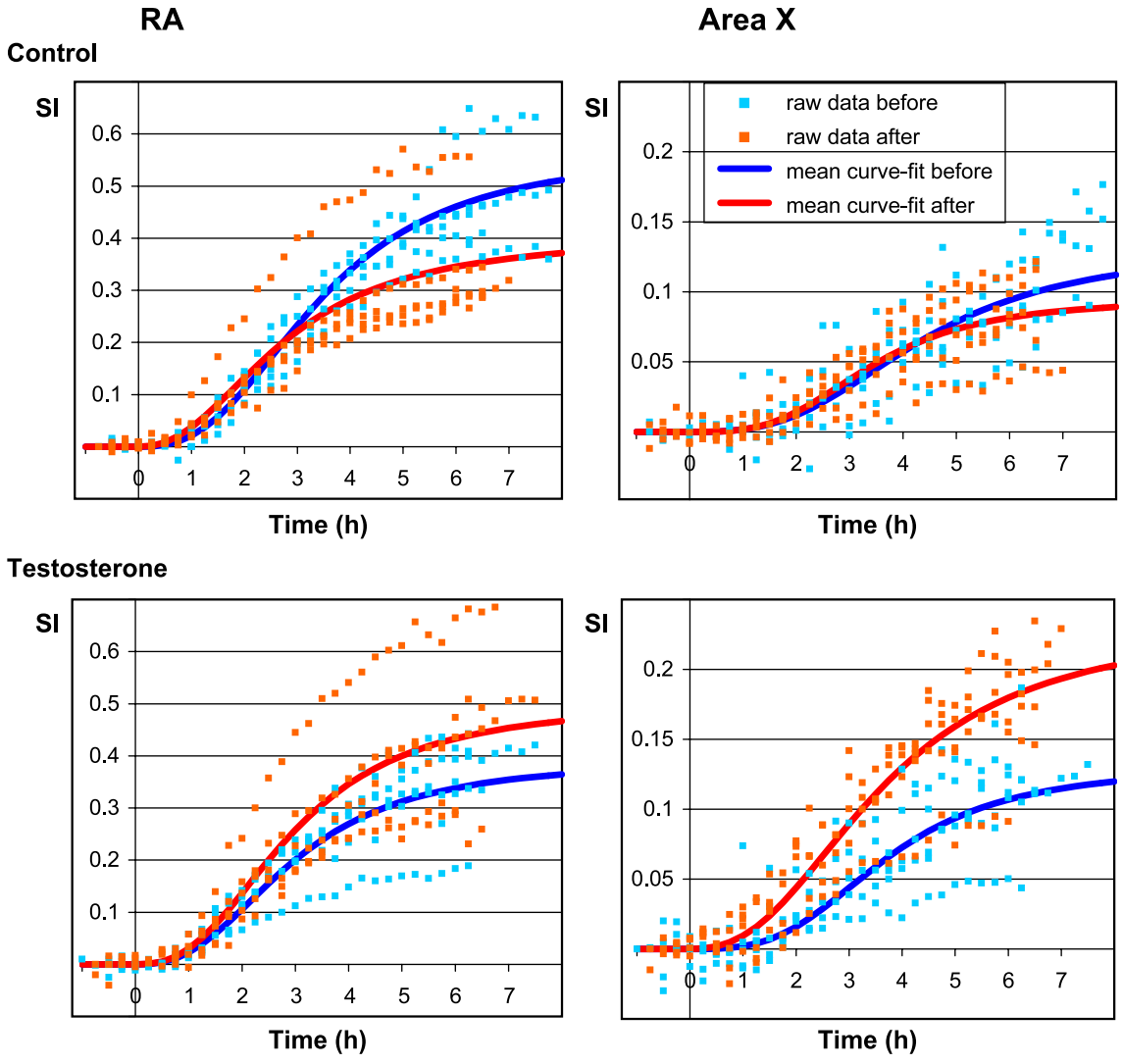

Fig. 4. Reconstruction of the sigmoid curves based on the mean parameter values in each group. The two rows show the raw data obtained from two repeated measurements in 10 animals along with the mean sigmoid fits through the data points obtained in control (top) and testosterone-treated (bottom) birds which illustrate the changes in the parameters SI_{max}, n and T_{50}. In area X testosterone-treatment causes a significant decrease in parameter n while T_{50} (the time at which half of SI_{max} is reached) did not change. The curve indicates that Mn^{2+} is accumulated faster in area X and that more Mn^{2+} is ultimately transported towards area X after testosterone-treatment than before.

the two groups of subjects resulting in a significant interaction between the two factors in the corresponding ANOVA. The two curves had fairly similar shapes in control and testosterone-treated birds before the endocrine treatments (see average n values in Fig. 3 and shapes of the curves in Fig. 4) but following testosterone application, the curve became much steeper in testosterone-treated birds to reach a higher asymptote (SI_{max}) in a similar amount of time. This is reflected in the significant interaction mentioned above. No difference in the half time (T_{50}) needed to reach the maximal intensities was detected in area X like in RA.

Total amount of Mn^{2+} accumulated in RA and area X

The amount of Mn^{2+} ultimately transported from HVC to RA or area X as estimated from the product of SI_{max} by volume increased markedly in both nuclei in testosterone-treated birds but concomitantly decreased in control subjects. Two-way ANOVA of these data detected significant interactions between repeated measurements and experimental groups in both RA [$F(1,8) = 5.869$, $P = 0.0417$] and area X [$F(1,8) = 5.662$, $P = 0.0446$] but no overall effects of the two factors (groups and time) was present (see Fig. 3 and Table 1 for detail of statistical results).

Discussion

We present here the first morphological and functional study of song control nuclei based on multiple ME-MRI measurements in the same subjects that were implanted with a permanent cannula in HVC to allow repeated injections of $MnCl_2$ at the same location. Repeated visualization of RA and area X demonstrated significant volume increases in testosterone-treated birds by comparison with control subjects (significant interactions in the two-way ANOVA). Testosterone treatment also significantly altered the rate of Mn^{2+} accumulation in area X but not in RA indicating specific effects of the steroid on the two classes of HVC projection neurons identified based on their targets. Testosterone also increased the total amount of Mn^{2+} ultimately transported to RA and area X. Together these data confirm and extend morphological results that were expected based on previous histological techniques in other songbird species and reveal new functional consequences of the exposure to testosterone that appear to be specific to the area X-projecting neurons. They also clearly demonstrate the validity of the dynamic ME-MRI approach in a previously well-characterized neural model and therefore demonstrate its usefulness for the study of other experimental models.

Volumetric changes in the song control nuclei following testosterone treatment

The effects of exogenous testosterone in female songbirds are species-specific. Whereas testosterone has no effect on singing and song control nuclei volumes in adult female zebra finches (Adkins-Regan and Ascenzi, 1990; Arnold, 1980; Gurney, 1981), testosterone induces active singing behavior and more than doubles the volume of HVC and RA in female canaries (Brown and Bottjer, 1993; Nottebohm, 1980). Previous studies showed that testosterone-treatment significantly increases song behavior in female starlings (De Ridder et al., 2002; Eens, 1997; Hausberger et al., 1995) but, to our knowledge, effects of exogenous testosterone on the volume of these nuclei has not been studied in females of this species.

We found here by histological techniques that testosterone-treated females have numerically larger RA and area X than control birds but these differences failed to reach statistical significance due to high individual variation for the limited sample size. Because the technique allows repeated measures in the same subjects, MRI assessed these volumetric changes taking into account variable baseline levels in controls and detected in this way significant effects of testosterone (interactions between testosterone and the repeated measurement) on both RA and area X volumes. The volume increase observed in testosterone-treated birds was paralleled by a decrease of similar amplitude in controls possibly related to spontaneous seasonal changes or to the mild but chronic stress induced by captivity.

Independent of the origin of this decrease in controls, these results illustrate the power of repeated imaging by ME-MRI. Although histology revealed no group difference in RA and area X volumes, an effect of testosterone on the volume of these nuclei was demonstrated by the significant interaction between treatment and repeated measures. Effects of testosterone were superimposed to the effects of a nonidentified phenomenon leading to a substantial although not significant volume decrease in controls. The use of birds as their own control and of a parallel control group allowed us to detect effects of testosterone that would have gone unnoticed in a single histological measure. This clearly illustrates the value of repeated MRI as a tool for the study brain plasticity over time. This technique could similarly be used in the future to analyze the detailed relationships between changes in size of these nuclei and in singing behavior as well as in other model systems.

The effects of testosterone on the volumes of RA and area X could result from a direct action on neurons located within these nuclei but also from indirect effects of the steroid (Ball et al., 2002). Because HVC is monosynaptically connected to these two nuclei, their plasticity might depend on the action of steroid hormones on receptors in HVC. This mode of action appears to be especially important for area X which does not apparently express significant levels of sex steroid receptors contrary to RA which contains many androgen receptor-positive neurons (Ball et al., 2002).

Functional changes in the song control nuclei induced by testosterone

ME-MRI also provided a measure of functional changes in response to testosterone in the two distinct projection pathways emerging from HVC. Mn^{2+} uptake into living cells is activity-dependent: Mn^{2+} is a calcium analogue that enters neurons via voltage-gated Ca^{2+} channels (Narita et al., 1990). Subsequent movements of Mn^{2+} are then mediated by fast axonal transport (Sloot and Gramsbergen, 1994) as confirmed by estimates of the speed of this process previously obtained in starlings and other species (Pautler et al., 1998; Van der Linden et al., 2002). Previous ME-MRI studies in mice, rats and monkeys showed that Mn^{2+} is released at the synapse and taken up by the postsynaptic neuron in the circuit (Pautler et al., 1998; Saleem et al., 2002). The Mn^{2+} transport therefore provides an effective tract-tracing method for in vivo MRI studies.

Mn^{2+} uptake is largely controlled by the electrical activity of the neuronal perikarya accumulating this ion. Based on available knowledge, it appears that the rate of Mn^{2+} transport along the axon is not very variable in physiological conditions and is only

affected in pathological states (anoxia, temperature changes) or following very deep anesthesia (Grafstein and Forman, 1980; Vallee and Bloom, 1991). This suggests that changes in the accumulation of Mn^{2+} in target nuclei reflect in a fairly direct manner the activity of the neurons where Mn^{2+} was injected and taken up. This technique was indeed used previously to visualize changes in the activity of the olfactory pathway in mice (Pautler and Koretsky, 2002). Acute exposure of mice to different odors affected the accumulation of Mn^{2+} in specific areas of the olfactory bulbs and in connected brain areas. The Mn^{2+} accumulation in these brain areas was also impaired in a dose-dependent manner by a calcium channel blocker thus confirming the notion that Mn^{2+} enters active neurons through calcium channels. In agreement with these data collected in mammals, the dynamics of Mn^{2+} accumulation in RA and area X following injection in HVC is modified in male canaries exposed to conspecific songs (Tindemans et al., 2003) and the dynamics of Mn^{2+} accumulation in RA and area X is different in male and female starlings reflecting the sexually differentiated activity and density of HVC neurons and their projections (Van der Linden et al., 2002). Together these results support to the notion that the dynamics of Mn^{2+} accumulation in a given nucleus reflects the activity/density of its synaptic inputs. Dynamic ME-MRI thus provides a new method to assess the functional state of a specific brain circuit that complements previously used techniques such as the analysis of immediate early genes expression or of 2-deoxyglucose uptake.

Since the two pathways emerging from HVC start from distinct populations of neurons within HVC, effects of testosterone on Mn^{2+} accumulation in RA and area X must be specifically related to the uptake or transport in these two separate pathways. There is, to our knowledge, no data available on the potential effects of testosterone on the rate of axonal transport but given that this aspect of the cellular physiology is very stable as long as the neuron is not placed in a pathological state (see above), it is likely that changes in axonal transport play no or only a minor role in the effects described here. Changes in the dynamics of Mn^{2+} accumulation in area X or in RA should therefore be directly related to the electrical activity of HVC neurons projecting to these nuclei and/or the density of their projections.

The increase in total amount of Mn^{2+} accumulated after 8 h (SI_{max} × volume) provides indirect experimental evidence demonstrating that testosterone significantly affects the basal activity, density or morphology of the connections between HVC and its monosynaptic targets, RA and area X. Its increase in both nuclei partially reflects the increase in the volume of these nuclei. However if no change in activity or density of HVC neurons and their projections had taken place, a same amount of Mn^{2+} would have accumulated in a larger volume thus resulting in lower SI_{max} values.

In addition to these global changes in the amounts of Mn^{2+} accumulated in the targets, specific changes in SI_{max} and in the *n* factor describing the rate of Mn^{2+} accumulation (the shape of the sigmoid curve) were detected in area X indicating specific effects of testosterone on this projection of HVC. In contrast, testosterone did not affect Mn^{2+} accumulation kinetics in RA suggesting that electrical activity in RA-projecting HVC neurons was not affected by testosterone. Several mechanisms could contribute to these differential effects of testosterone on the HVC projections towards RA and area X. Three types of explanations deserve special consideration.

It must first be reminded that in the HVC of songbirds, the RA projection neurons are replaced at high rate during the annual cycle while there is no replacement of area X projecting cells (Alvarez-Buylla and Kirn, 1997). The replacement of RA projecting neurons is controlled by testosterone, which significantly increases the rate of neuronal incorporation when present in high level in the plasma (Rasika et al., 1994). It can therefore be expected that the testosterone-treated female starlings experienced during the experiment a large increase in the number of RA-projecting HVC neurons while the number of area X projecting neurons remained unchanged. This could explain the increase in the total amount (SI_{max} × volume) of Mn^{2+} transported to RA (increase in the number of HVC neurons and/or of their projections to RA) but not to area X. It is actually puzzling to notice that the SI_{max} increased in area X but not in the RA pathway. This surprising observation must find its explanation either in the endocrine characteristics or in the electrophysiological characteristics of these two types of HVC neurons.

A second explanation of these specific changes in Mn^{2+} accumulation could be related to differences in steroid receptors types expressed by the two types of HVC projection neurons. Neurons projecting to RA only express androgen receptors whereas the neurons that project to area X contain both androgen and estrogen receptors of the alpha subtype (Bernard et al., 1999; Johnson and Bottjer, 1995; Sohrabji et al., 1989). Testosterone is converted into estrogen by the enzyme aromatase in the telencephalon of songbirds, mainly in the medial part of the caudal neostriatum (Balthazart et al., 1996; Metzdorf et al., 1999; Saldanha et al., 2000; Shen et al., 1995; Vockel et al., 1990). Testosterone entering the brain could thus be converted into estrogens in neurons located within the caudal neostriatum and then be released by aromatase-positive terminals in the vicinity of HVC. Aromatase activity is increased by testosterone in female canaries (Fusani et al., 2001) and shows a seasonal peak during the early spring in adult male starlings when plasma testosterone is maximal (Riters et al., 2001). The treatment with testosterone of female starlings thus probably increased available estrogens in HVC and these estrogens could be responsible for the specific increase in activity of area X-projecting HVC neurons, RA-projecting neurons being unaffected because they do not express estrogen receptors. The present study would then suggest that estrogen action could be linked more specifically to the modulation of the anterior forebrain pathway implicated in the control of song learning and song stability. This hypothesis could be tested by repeated ME-MRI in birds submitted to treatments specifically affecting the availability of estrogens or nonaromatizable androgens in the brain such as the injection of estradiol or 5α-dihydrotestosterone or the treatment with testosterone in association with an aromatase inhibitor.

Thirdly and finally, electrophysiological characteristics of the two types of HVC projection neurons and of the specific interneurons that modulate their activity could play a key role in determining the differential effects of testosterone on the Mn^{2+} accumulation in RA and area X. Recent electrophysiological studies indicate that hearing their own song evokes in songbirds interneuronal firing that closely matches the responses evoked by the same stimuli in area X projecting neurons, suggesting that HVC interneurons make restricted inputs onto area X-projecting (but not on RA projecting) neurons (Mooney, 2000). In addition, it has been reported that a particular type of action potential waveforms (short potential duration and high firing rate) is observed more frequently in breeding than in nonbreeding male canaries (Del Negro and Edeline, 2002). These action potentials character-

istics are usually associated with interneurons suggesting that interneurons may be more active and/or more numerous in breeding birds, i.e., in conditions associated with high plasma testosterone levels. Because the activity of these neurons has been found to be closely associated with the activity of area X projecting neurons (Mooney, 2000), it can thus be speculated that the changes in the activity and Mn^{2+} transport in area X-projecting neurons results from effects of testosterone on the activity and the number of interneurons that innervate them. In any case, it cannot, contrary to what is observed in RA, reflect changes in the numbers of area-X projecting HVC neurons since these are known to be present in stable numbers in adult songbirds.

Future experiments with ME-MRI on the song control system will be carried out in combination with other recently developed MRI techniques such as diffusion weighted and diffusion tensor imaging, which allow quantification of cell density and connectivity of the brain regions involved. In addition, MRI studies could be combined with histological techniques such as the labeling of dividing neurons by bromo-deoxyuridine or the assessment of neuronal connectivity between HVC and its target by tract tracing to better discriminate between effects due to changes in the morphological substrate of the neuronal circuit or in its functional properties.

In conclusion, the dynamic ME-MRI confirmed here many morphological and physiological effects of testosterone in one of the best characterized neuronal circuits in warm-blooded vertebrates. This technique also revealed new features of the global activity in this system that would have been difficult if not impossible to identify by previously available techniques such as electrophysiology or 2-deoxyglucose autoradiography. Functional changes were detected in subpopulations of HVC neurons that can be univocally identified by their connections to specific targets. These results reflect either the changes in neuron numbers that are known to be induced by exposure to testosterone and/or changes in neuronal activity confined to specific neuronal populations. Dynamic ME-MRI therefore represents a new technique for the neurosciences that can be used to address a variety of questions concerning the physiology and plasticity of precisely identified brain circuits.

Acknowledgments

This research was supported by grants from the National Science Foundation (FWO, project No. G.0075.98N and G.0420.02) and BOF-NOI and RAFO funds from the University of Antwerp to AVdL, and by grants from the NINDS (NS 35467), the Belgian FRFC (Nbr. 2.4555.01), and the Government of the French Community of Belgium (ARC #99/044-241) to JB. PA is postdoctoral researcher with the National Science Foundation (FWO) Flanders. VVM is grant holder from the Institute for the Promotion of Innovation by Science and Technology in Flanders (IWT-V).

References

Adkins-Regan, E., Ascenzi, M., 1990. Sexual differentiation of behavior in the zebra finch: effect of early gonadectomy or androgen treatment. Horm. Behav. 24, 114–127.

Alvarez-Buylla, A., Kirn, J.R., 1997. Birth, migration, incorporation, and death of vocal control neurons in adult songbirds. J. Neurobiol. 33, 585–601.

Aoki, I., Tanaka, C., Takegami, T., Ebisu, T., Umeda, M., Fukunaga, M., Fukuda, K., Silva, A.C., Koretsky, A.P., Naruse, S., 2002. Dynamic activity-induced manganese-dependent contrast magnetic resonance imaging (DAIM MRI). Magn. Reson. Med. 48, 927–933.

Arnold, A.P., 1980. Effects of androgens on volumes of sexually dimorphic brain regions in the zebra finch. Brain Res. 185, 441–444.

Ball, G.F., Wingfield, J.C., 1987. Changes in plasma levels of luteinizing-hormone and sex steroid hormones in relation to multiple-broodedness and nest-site density in male starlings. Physiol. Zool. 60, 191–199.

Ball, G.F., Riters, L.V., Balthazart, J., 2002. Neuroendocrinology of song behavior and avian brain plasticity: multiple sites of action of sex steroid hormones. Front. Neuroendocrinol. 23, 137–178.

Balthazart, J., Absil, P., Foidart, A., Houbart, M., Harada, N., Ball, G.F., 1996. Distribution of aromatase-immunoreactive cells in the forebrain of zebra finches (*Taeniopygia guttata*): implications for the neural action of steroids and nuclear definition in the avian hypothalamus. J. Neurobiol. 31, 129–148.

Bernard, D.J., Bentley, G.E., Balthazart, J., Turek, F.W., Ball, G.F., 1999. Androgen receptor, estrogen receptor alpha, and estrogen receptor beta show distinct patterns of expression in forebrain song control nuclei of European starlings. Endocrinology 140, 4633–4643.

Brainard, M.S., Doupe, A.J., 2000a. Interruption of a basal ganglia–forebrain circuit prevents plasticity of learned vocalizations. Nature 404, 762–766.

Brainard, M.S., Doupe, A.J., 2000b. Auditory feedback in learning and maintenance of vocal behaviour. Nat. Rev., Neurosci. 1, 31–40.

Brenowitz, E.A., Margoliash, D., Nordeen, K.W., 1997. An introduction to birdsong and the avian song system. J. Neurobiol. 33, 495–500.

Brown, S.D., Bottjer, S.W., 1993. Testosterone-induced changes in adult canary brain are reversible. J. Neurobiol. 24, 627–640.

De Ridder, E., Pinxten, R., Mees, V., Eens, M., 2002. Short- and long-term effects of male-like concentrations of testosterone on female European starlings (*Sturnus vulgaris*). Auk 119, 487–497.

Del Negro, C., Edeline, J.M., 2002. Sex and season influence the proportion of thin spike cells in the canary HVC. NeuroReport 13, 2005–2009.

Duffy, D.L., Bentley, G.E., Drazen, D.L., Ball, G.F., 2000. Effects of testosterone on cell-mediated and humoral immunity in non-breeding adult European starlings. Behav. Ecol. 11, 654–662.

Duong, T.Q., Silva, A.C., Lee, S.P., Kim, S.G., 2000. Functional MRI of calcium-dependent synaptic activity: cross correlation with CBF and BOLD measurements. Magn. Reson. Med. 43, 383–392.

Eens, M., 1997. Understanding the complex song of the European starling: an integrated ethological approach. Adv. Study Behav. 26, 355–434.

Eens, M., Van Duyse, E., Berghman, L., Pinxten, R., 2000. Shield characteristics are testosterone-dependent in both male and female moorhens. Horm. Behav. 37, 126–134.

Fusani, L., Hutchison, J.B., Gahr, M., 2001. Testosterone regulates the activity and expression of aromatase in the canary neostriatum. J. Neurobiol. 49, 1–8.

Grafstein, B., Forman, D.S., 1980. Intracellular transport in neurons. Physiol. Rev. 60, 1167–1283.

Gurney, M.E., 1981. Hormonal control of cell form and number in the zebra finch song system. J. Neurosci. 1, 658–673.

Hausberger, M., Henry, L., Richard, M.A., 1995. Testosterone-induced singing in female European starlings (*Sturnus vulgaris*). Ethology 99, 193–208.

Hessler, N.A., Doupe, A.J., 1999. Singing-related neural activity in a dorsal forebrain–basal ganglia circuit of adult zebra finches. J. Neurosci. 19, 10461–10481.

Jarvis, E.D., Scharff, C., Grossman, M.R., Ramos, J.A., Nottebohm, F., 1998. For whom the bird sings: context-dependent gene expression. Neuron 21, 775–788.

Johnson, F., Bottjer, S.W., 1995. Differential estrogen accumulation among

populations of projection neurons in the higher vocal center of male canaries. J. Neurobiol. 26, 87–108.
Lin, Y.J., Koretsky, A.P., 1997. Manganese ion enhances T1-weighted MRI during brain activation: an approach to direct imaging of brain function. Magn. Reson. Med. 38, 378–388.
Metzdorf, R., Gahr, M., Fusani, L., 1999. Distribution of aromatase, estrogen receptor, and androgen receptor mRNA in the forebrain of songbirds and nonsongbirds. J. Comp. Neurol. 407, 115–129.
Mooney, R., 2000. Different subthreshold mechanisms underlie song selectivity in identified HVc neurons of the zebra finch. J. Neurosci. 20, 5420–5436.
Mooney, R., Rosen, M.J., Sturdy, C.B., 2002. A bird's eye view: top down intracellular analyses of auditory selectivity for learned vocalisations. J. Comp. Physiol., A 188, 879–895.
Narita, K., Kawasaki, F., Kita, H., 1990. Mn and Mg influxes through Ca channels of motor nerve terminals are prevented by verapamil in frogs. Brain Res. 510, 289–295.
Nottebohm, F., 1980. Testosterone triggers growth of brain vocal control nuclei in adult female canaries. Brain Res. 189, 429–436.
Nottebohm, F., Stokes, T.M., Leonard, C.M., 1976. Central control of song in the canary, *Serinus canarius*. J. Comp. Neurol. 165, 457–486.
Pautler, R.G., Koretsky, A.P., 2002. Tracing odor-induced activation in the olfactory bulbs of mice using manganese-enhanced magnetic resonance imaging. NeuroImage 16, 441–448.
Pautler, R.G., Silva, A.C., Koretsky, A.P., 1998. In vivo neuronal tract tracing using manganese-enhanced magnetic resonance imaging. Magn. Reson. Med. 40, 740–748.
Rasika, S., Nottebohm, F., Alvarez-Buylla, A., 1994. Testosterone increases the recruitment and/or survival of new high vocal center neurons in adult female canaries. Proc. Natl. Acad. Sci. 91, 7854–7858.
Riters, L.V., Baillien, M., Eens, M., Pinxten, R., Foidart, A., Ball, G.F., Balthazart, J., 2001. Seasonal variation in androgen-metabolizing enzymes in the diencephalon and telencephalon of the male European starling (*Sturnus vulgaris*). J. Neuroendocrinol. 13, 985–997.
Saldanha, C.J., Tuerk, M.J., Kim, Y.H., Fernandes, A.O., Arnold, A.P., Schlinger, B.A., 2000. Distribution and regulation of telencephalic aromatase expression in the zebra finch revealed with a specific antibody. J. Comp. Neurol. 423, 619–630.
Saleem, K.S., Pauls, J.M., Augath, M., Trinath, T., Prause, B.A., Hashikawa, T., Logothetis, N.K., 2002. Magnetic resonance imaging of neuronal connections in the macaque monkey. Neuron 34, 685–700.
Scharff, C., Nottebohm, F., 1991. A comparative study of the behavioral deficits following lesions of various parts of the zebra finch song system: implications for vocal learning. J. Neurosci. 11, 2896–2913.
Shen, P., Schlinger, B.A., Campagnoni, A.T., Arnold, A.P., 1995. An atlas of aromatase mRNA expression in the zebra finch brain. J. Comp. Neurol. 360, 172–184.
Sloot, W.N., Gramsbergen, J.B., 1994. Axonal transport of manganese and its relevance to selective neurotoxicity in the rat basal ganglia. Brain Res. 657, 124–132.
Sohrabji, F., Nordeen, K.W., Nordeen, E.J., 1989. Projections of androgen-accumulating neurons in a nucleus controlling avian song. Brain Res. 488, 253–259.
Steel, R.G.D., Torrie, J.H., 1980. Principles and Procedures of Statistics. A Biometrical Approach, second ed. McGraw-Hill Book Company, New York. 633 pp.
Tindemans, I., Verhoye, M., Balthazart, J., Van der Linden, A., 2003. In vivo dynamic ME-MRI reveals differential functional responses of RA- and area X-projecting neurones in the HVC of canaries exposed to conspecific song. Eur. J. Neurosci. 18, 1–9.
Tramontin, A.D., Brenowitz, E.A., 2000. Seasonal plasticity in the adult brain. Trends Neurosci. 23, 251–258.
Vallee, R.B., Bloom, G.S., 1991. Mechanisms of fast and slow axonal transport. Annu. Rev. Neurosci. 14, 59–92.
Van der Linden, A., Verhoye, M., Van Meir, V., Tindemans, I., Eens, M., Absil, P., Balthazart, J., 2002. In vivo manganese-enhanced magnetic resonance imaging reveals connections and functional properties of the songbird vocal control system. Neuroscience 112, 467–474.
Vockel, A., Prove, E., Balthazart, J., 1990. Effects of castration and testosterone treatment on the activity of testosterone-metabolizing enzymes in the brain of male and female zebra finches. J. Neurobiol. 21, 808–825.
Wild, J.M., 1997. Neural pathways for the control of birdsong production. J. Neurobiol. 33, 653–670.
Yu, A.C., Margoliash, D., 1996. Temporal hierarchical control of singing in birds. Science 273, 1871–1875.